

Significant consequences of heat generation/absorption and homogeneous-heterogeneous reactions in second grade fluid due to rotating disk



Tasawar Hayat^{a,b}, Sumaira Qayyum^{a,*}, Ahmed Alsaedi^b, Bashir Ahmad^b

^a Department of Mathematics, Quaid-I-Azam University, 45320 Islamabad 44000, Pakistan

^b Nonlinear Analysis and Applied Mathematics (NAAM) Research Group, Department of Mathematics, Faculty of Science, King Abdulaziz University, Jeddah 21589, Saudi Arabia

ARTICLE INFO

Article history:

Received 2 November 2017
Received in revised form 22 November 2017
Accepted 7 December 2017
Available online 11 December 2017

Keywords:

Stretchable rotating disk
Second grade fluid
Heat generation/absorption
Homogeneous-heterogeneous reactions

ABSTRACT

Flow of second grade fluid by a rotating disk with heat and mass transfer is discussed. Additional effects of heat generation/absorption are also analyzed. Flow is also subjected to homogeneous-heterogeneous reactions. The convergence of computed solution is assured through appropriate choices of initial guesses and auxiliary parameters. Investigation is made for the effects of involved parameters on velocities (radial, axial, tangential), temperature and concentration. Skin friction and Nusselt number are also analyzed. Graphical results depict that an increase in viscoelastic parameter enhances the axial, radial and tangential velocities. Opposite behavior of temperature is observed for larger values of viscoelastic and heat generation/absorption parameters. Concentration profile is increasing function of Schmidt number, viscoelastic parameter and heterogeneous reaction parameter. Magnitude of skin friction and Nusselt number are enhanced for larger viscoelastic parameter.

© 2018 The Authors. Published by Elsevier B.V. This is an open access article under the CC BY-NC-ND license (<http://creativecommons.org/licenses/by-nc-nd/4.0/>).

Introduction

Non-Newtonian fluids have extensive applications in technological and industrial sectors. Formulation of equations for these types of fluids is complex in comparison to the usual Navier Stokes equation. It is due to extra rheological parameters in the constitutive relations of such materials. Applications related to geophysics, biological sciences and chemical processes involve non-Newtonian materials. Materials such as foams, pastes, ketchup, lubricant, certain oils, sugar solution, apple sauce, colloidal and suspension solutions, drilling muds, clay coating and soaps are the non-Newtonian fluids. Stagnation point flow of tangent hyperbolic nanofluid with nonlinear thermal radiation and double diffusive convection is examined by Hayat et al. [1]. Flow of micropolar fluid due to heated stretching sheet is analyzed by Turkyilmazoglu [2]. Rotating flow of Jeffrey fluid for Cattaneo-Christov heat flux is presented by Hayat et al. [3]. Rahman et al. [4] analyzed the effect of slip on flow of Jeffrey nanofluid through tapered artery with mild stenosis. Hayat et al. [5] studied the MHD flow of Jeffrey fluid accounting constructive and destructive chemical reactions. Das et al. [6] explored the heat/mass transfer of sec-

ond grade fluid over a stretching sheet. Hayat et al. [7] analyzed the squeezing flow of second grade fluid with convective boundary conditions. Consequences of Soret/Dufour effects on flow of second grade fluid due to stretching cylinder are discussed by Majeed et al. [8]. Hayat et al. [9] examined the flow of second grade fluid in thermally stratified medium with non-Fourier heat flux. Ariel [10] studied the flow of second grade fluid by a rotating disk.

At present many researchers and scientists are considering flow problems due to rotating surfaces. It is due to its significance in engineering and industrial sectors involving electric power generating system, jet motors, turbine system and food processing. Karman [11] employed transformations in obtaining ordinary differential system for rotating disk flow by Navier Stokes equations. Cochran [12] used these transformations to analyze the rotating disk flow by numerical integration method. Stewartson [13] considered the flow between two rotating disks. Flow between stationary and rotating disks is examined by Chapple and Stokes [14]. Flow between rotating disks with thermal stratification is described by Hayat et al. [15]. Ellahi et al. [16] examined ferrofluid flow by stretchable rotating disk. Flow due to stretchable rotating disks with Cattaneo-Christov heat flux is addressed by Hayat et al. [17].

When there exists high temperature difference between the ambient fluid and surface then effects of heat source/sink are use-

* Corresponding author.

E-mail address: sumaira@math.qau.edu.pk (S. Qayyum).

ful. Heat generation works in exothermic or endothermic chemical reactions. Raju and Sandeep [18] considered heat source/sink effects in flow of Casson fluid. Effects of heat source/sink in flow of nanofluid over shrinking sheet is analyzed by Das et al. [19]. Radiative flow of nanofluid in presence of an inclined MHD and heat generation/absorption is explored by Hayat et al. [20]. MHD flow by an inclined permeable sheet is examined by Noor et al. [21]. Aziz [22] studied stagnation point flow in presence of heat source/sink.

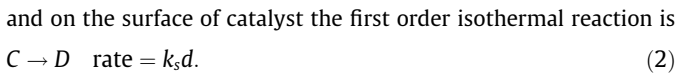
It should be noted that several chemical reacting systems consist of homogeneous-heterogeneous reactions. Except in the presence of catalyst some of the reactions does not work or may proceed very slow. Correlation between homogeneous-heterogeneous reactions is very complex. Ceramics, fog dispersion, food processing, crops damage via freezing, fog formation and polymer production, hydrometallurgical industry are applications of chemical reaction. Various scientists now are now engaged in the discussion of flows with homogeneous-heterogeneous different aspects [23–27].

Existing literature survey witnesses that flow of second grade fluid by stretchable rotating disks with homogeneous-heterogeneous reactions is not yet studied. Effects of heat generation absorption is also considered. The objective here is to carry out such analysis. Convergent series solutions are developed through HAM [28–36]. Plots explore the outcome of sundry variables for the velocity, temperature, concentration, skin friction coefficient and Nusselt number. Important points are concluded.

Modeling

Consider the steady axisymmetric flow of second grade fluid by a rotating disk. Disk at $z = 0$ rotate with angular velocity Ω_1 . Stretching rate of disk is a_1 . Disk and ambient temperatures are maintained at \hat{T}_w and \hat{T}_∞ respectively (see Fig. 1).

Effects of heat generation/absorption are considered. Homogeneous-heterogeneous reactions are also present. Homogeneous reaction for cubic autocatalysis is



Here k_c and k_s are the rate constants and C and D are chemical species with concentrations c and d . We have used the cylindrical coordinates (r, θ, z) with velocity components $(\hat{u}, \hat{v}, \hat{w})$. The relevant equations are

$$\frac{\partial \hat{u}}{\partial r} + \frac{\hat{u}}{r} + \frac{\partial \hat{w}}{\partial z} = 0, \tag{3}$$

$$\begin{aligned} \hat{u} \frac{\partial \hat{u}}{\partial r} + \hat{w} \frac{\partial \hat{u}}{\partial z} - \frac{\hat{v}^2}{r} = & \nu \frac{\partial^2 \hat{u}}{\partial z^2} + \frac{\alpha_1}{\rho} \left(\hat{u} \frac{\partial^3 \hat{u}}{\partial r \partial z^2} + \hat{w} \frac{\partial^3 \hat{u}}{\partial z^3} + \frac{\partial \hat{v}}{\partial r} \frac{\partial^2 \hat{v}}{\partial z^2} \right. \\ & - \frac{1}{r} \left(\frac{\partial \hat{u}}{\partial z} \right)^2 - \frac{\partial^2 \hat{v}}{\partial z^2} \frac{\hat{v}}{r} + \frac{\partial \hat{v}}{\partial z} \frac{\partial^2 \hat{v}}{\partial r \partial z} + \frac{\partial \hat{w}}{\partial z} \frac{\partial^2 \hat{u}}{\partial z^2} \\ & \left. + 3 \frac{\partial \hat{u}}{\partial z} \frac{\partial^2 \hat{u}}{\partial r \partial z} + 2 \frac{\partial \hat{u}}{\partial r} \frac{\partial^2 \hat{u}}{\partial z^2} \right) \end{aligned} \tag{4}$$

$$\begin{aligned} \hat{u} \frac{\partial \hat{v}}{\partial r} + \hat{w} \frac{\partial \hat{v}}{\partial z} + \frac{\hat{u} \hat{v}}{r} \\ = \nu \frac{\partial^2 \hat{v}}{\partial z^2} + \frac{\alpha_1}{\rho} \left(\hat{u} \frac{\partial^3 \hat{v}}{\partial r \partial z^2} + \hat{w} \frac{\partial^3 \hat{v}}{\partial z^3} - 2 \frac{\partial \hat{v}}{\partial z} \frac{\partial^2 \hat{u}}{\partial r \partial z} + \frac{\partial^2 \hat{v}}{\partial z^2} \frac{\hat{u}}{r} - \frac{1}{r} \frac{\partial \hat{u}}{\partial z} \frac{\partial \hat{v}}{\partial z} \right) \end{aligned} \tag{5}$$

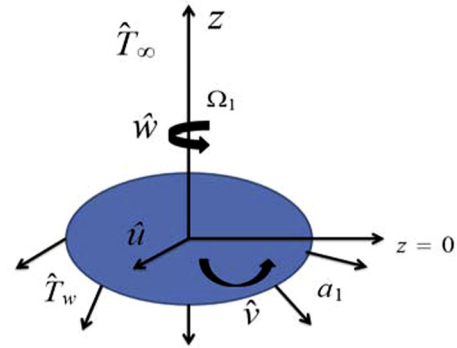


Fig. 1. Flow geometry.

$$(\rho c_p) \left(\hat{u} \frac{\partial \hat{T}}{\partial r} + \hat{w} \frac{\partial \hat{T}}{\partial z} \right) = k \frac{\partial^2 \hat{T}}{\partial z^2} + Q^* (\hat{T} - \hat{T}_\infty), \tag{6}$$

$$\hat{u} \frac{\partial c}{\partial r} + \hat{w} \frac{\partial c}{\partial z} = D_c^* \left(\frac{\partial^2 c}{\partial r^2} + \frac{1}{r} \frac{\partial c}{\partial r} + \frac{\partial^2 c}{\partial z^2} \right) - k_c c d^2, \tag{7}$$

$$\hat{u} \frac{\partial d}{\partial r} + \hat{w} \frac{\partial d}{\partial z} = D_d^* \left(\frac{\partial^2 d}{\partial r^2} + \frac{1}{r} \frac{\partial d}{\partial r} + \frac{\partial^2 d}{\partial z^2} \right) + k_c c d^2, \tag{8}$$

with boundary conditions

$$\begin{aligned} \hat{u} = r a_1, \quad \hat{v} = r \Omega_1, \quad \hat{w} = 0, \quad \hat{T} = \hat{T}_w, \quad D_c^* \frac{\partial c}{\partial z} = k_s c, \\ D_d^* \frac{\partial d}{\partial z} = -k_s c \text{ at } z = 0, \\ \hat{u} = 0, \quad \hat{v} = 0, \quad \hat{w} = 0, \quad \hat{T} = \hat{T}_\infty, \quad c \rightarrow c_0, \quad d \rightarrow 0 \text{ at } z \rightarrow \infty, \end{aligned} \tag{9}$$

where α_1 is material parameter of second grade fluid, ρ density, c_p specific heat, k thermal conductivity, ν kinematic viscosity, Q^* heat generation absorption coefficient and D_c^* and D_d^* are diffusion species coefficients. Letting [15]:

$$\begin{aligned} \hat{u} = r \Omega_1 \tilde{f}'(\xi), \quad \hat{v} = r \Omega_1 \tilde{g}(\xi), \quad \hat{w} = -2h \Omega_1 \tilde{f}(\xi), \quad \tilde{\theta} = \frac{\hat{T} - \hat{T}_\infty}{\hat{T}_w - \hat{T}_\infty}, \\ \tilde{p} = \rho_f \Omega_1 \nu_f \left(P(\xi) + \frac{1}{2} \frac{r^2}{h^2} \epsilon \right), \quad c = c_0 \tilde{\phi}, \quad d = c_0 \tilde{l}, \quad \xi = \frac{z}{h}, \end{aligned} \tag{10}$$

the continuity equation is satisfied and Eqs. (4)–(9) are reduced to

$$\tilde{f}''' + \text{WeRe} (2\tilde{f}''^2 + \tilde{g}'^2 - 2\tilde{f}\tilde{f}'' + \tilde{f}\tilde{f}''') - \text{Re}(\tilde{f}'^2 - 2\tilde{f}\tilde{f}'' - \tilde{g}'^2) = 0, \tag{11}$$

$$\tilde{g}'' + \text{WeRe} (2\tilde{f}'\tilde{g}'' - 2\tilde{f}\tilde{g}''' - 3\tilde{f}''\tilde{g}') - \text{Re}(2\tilde{f}'\tilde{g} - 2\tilde{f}\tilde{g}') = 0, \tag{12}$$

$$\tilde{\theta}'' + \text{PrRe}(\tilde{f}'\tilde{\theta} - 2\tilde{f}\tilde{\theta}' + Q\tilde{\theta}) = 0, \tag{13}$$

$$\frac{1}{\text{Re}} \frac{1}{\text{Sc}} \tilde{\phi}'' + 2\tilde{f}\tilde{\phi}' - k_1 \tilde{\phi} \tilde{l}^2 = 0, \tag{14}$$

$$\frac{\delta}{\text{Sc}} \frac{1}{\text{Re}} \tilde{l}'' + 2\tilde{f}\tilde{l}' + k_1 \tilde{\phi} \tilde{l}^2 = 0, \tag{15}$$

with

$$\begin{aligned} \tilde{f}(0) = 0, \quad \tilde{f}(\infty) = 0, \quad \tilde{f}'(0) = A_1, \quad \tilde{f}'(\infty) = 0, \quad \tilde{g}(0) = 1, \\ \tilde{g}(\infty) = 0, \quad \tilde{\theta}(0) = 1, \quad \tilde{\theta}(\infty) = 0, \quad \tilde{\phi}'(0) = k_2 \tilde{\phi}(0), \quad \tilde{\phi}(\infty) = 1, \\ \delta \tilde{l}'(0) = -k_2 \tilde{\phi}(0), \quad \tilde{l}(\infty) = 0, \quad P(0) = 0, \end{aligned} \tag{16}$$

$$\begin{aligned}
 \text{Re} &= \frac{\Omega_1 h^2}{\nu}, A_1 = \frac{a_1}{\Omega_1}, \text{We} = \frac{\alpha_1}{\rho h^2} \\
 \text{Pr} &= \frac{\rho c_p \nu}{k}, Q = \frac{Q^*}{\rho c_p \Omega_1}, k_1 = \frac{k_c c_0^2}{\Omega_1} \\
 k_2 &= \frac{k_s h}{D_c^*}, \delta = \frac{D_D^*}{D_c^*}, \text{Sc} = \frac{\nu}{D_c^*},
 \end{aligned}
 \tag{17}$$

Here Re denotes Reynolds number, A_1 stretching parameter, We Weissenberg number, Pr Prandtl number, Q_0 heat generation/absorption parameter, k_1 and k_2 the homogeneous and heterogeneous reaction parameters respectively, δ ratio of diffusion coefficient and Sc Schmidt number. When diffusion coefficients D_c^* and D_D^* are equal for both chemical species i.e. $\delta = 1$ then

$$\tilde{\phi}(\xi) + \tilde{I}(\xi) = 1.
 \tag{18}$$

Now Eqs. (14) and (15) yield

$$\frac{1}{\text{Re}} \frac{1}{\text{Sc}} \tilde{\phi}'' + 2\tilde{f}\tilde{\phi}' - k_1\tilde{\phi}(1 - \tilde{\phi})^2 = 0,
 \tag{19}$$

with boundary conditions

$$\tilde{\phi}'(0) = k_2\tilde{\phi}(0), \quad \tilde{\phi}(1) = 1.
 \tag{20}$$

Skin friction coefficients in radial and tangential directions are C_{f_r} and C_{f_θ} respectively

$$C_{f_r} = \frac{\tau_{zr}}{\rho(r\Omega_1)^2},
 \tag{21}$$

$$C_{f_\theta} = \frac{\tau_{z\theta}}{\rho(r\Omega_1)^2},
 \tag{22}$$

Shear stresses τ_{zr} and $\tau_{z\theta}$ are defined by

$$\begin{aligned}
 \tau_{zr} &= \mu \left(\frac{\partial u}{\partial z} + \frac{\partial w}{\partial r} \right) + \alpha_1 \left(u \frac{\partial}{\partial r} + w \frac{\partial}{\partial z} \right) \left(\frac{\partial u}{\partial z} + \frac{\partial w}{\partial r} \right) + 2 \frac{\partial v}{\partial z} \left(\frac{\partial v}{\partial r} - \frac{v}{r} \right) \\
 &+ \frac{\partial u}{\partial r} \frac{\partial w}{\partial r} + \frac{\partial u}{\partial z} \frac{\partial w}{\partial z} + 3 \left(\frac{\partial u}{\partial r} \frac{\partial u}{\partial z} + \frac{\partial w}{\partial r} \frac{\partial w}{\partial z} \right) \\
 &- \alpha_1 \left(\left(\frac{\partial u}{\partial r} + \frac{\partial w}{\partial z} \right) \left(\frac{\partial u}{\partial z} + \frac{\partial w}{\partial r} \right) + \frac{\partial v}{\partial z} \left(\frac{\partial v}{\partial r} - \frac{v}{r} \right) \right),
 \end{aligned}
 \tag{23}$$

$$\begin{aligned}
 \tau_{z\theta} &= \mu \frac{\partial v}{\partial z} \\
 &+ \alpha_1 \left(u \frac{\partial^2 v}{\partial r \partial z} + w \frac{\partial^2 v}{\partial z^2} + \frac{\partial u}{\partial z} \frac{\partial v}{\partial r} - \frac{v}{r} \frac{\partial u}{\partial z} + 3 \frac{u}{r} \frac{\partial v}{\partial z} + \frac{\partial v}{\partial z} \frac{\partial w}{\partial z} \right) \\
 &- \alpha_1 \left(\frac{\partial u}{\partial z} \frac{\partial v}{\partial r} - \frac{v}{r} \frac{\partial u}{\partial z} + \frac{\partial w}{\partial r} \frac{\partial v}{\partial r} - \frac{v}{r} \frac{\partial w}{\partial r} + 2 \frac{u}{r} \frac{\partial v}{\partial z} + 2 \frac{\partial v}{\partial z} \frac{\partial w}{\partial z} \right),
 \end{aligned}
 \tag{24}$$

Skin friction coefficients C_{f_r} and C_{f_θ} in dimensionless forms are

Table 1
Solutions convergence when $\text{Re} = 0.3, A_1 = 0.4, \text{We} = 0.01, \text{Pr} = 1.5, k_1 = k_2 = 0.4, \text{Sc} = 1$ and $Q = 0.2$.

Order of approximations	$\tilde{f}''(0)$	$-\tilde{g}'(0)$	$-\tilde{\theta}'(0)$	$\tilde{\phi}'(0)$
1	0.0044	0.4300	0.6120	0.17741
5	0.0259	0.5479	0.3467	0.16148
10	0.0150	0.5599	0.3158	0.16483
22	0.0150	0.5573	0.3095	0.16958
23	0.0150	0.5572	0.3096	0.16959
24	0.0150	0.5572	0.3097	0.16961
26	0.0150	0.5572	0.3099	0.16961
30	0.0150	0.5572	0.3099	0.16961
40	0.0150	0.5572	0.3099	0.16961

$$\text{Re} C_{f_r} = \tilde{f}''(0) + \beta \text{Re} [3\tilde{f}'(0)\tilde{f}''(0) - 2\tilde{f}(0)\tilde{f}'''(0) + \tilde{g}(0)\tilde{g}'(0)],
 \tag{25}$$

$$\text{Re} C_{f_\theta} = \tilde{g}'(0) + \beta \text{Re} [4\tilde{f}'(0)\tilde{g}'(0) - 2\tilde{f}(0)\tilde{g}''(0)],
 \tag{26}$$

where local Reynolds number is $\text{Re}_r = \frac{r\Omega_1 h}{\nu}$.

Heat transfer rate is defined as

$$\text{Nu}_x = \frac{h q_w}{k(\hat{T}_w - \hat{T}_\infty)} \Big|_{z=0},
 \tag{27}$$

in which wall heat flux q_w is given by

$$q_w|_{z=0} = -k \frac{\partial \hat{T}}{\partial z} \Big|_{z=0}.
 \tag{28}$$

Nusselt number is

$$\text{Nu}_x = -\tilde{\theta}'(0).
 \tag{29}$$

Solutions methodology and convergence

Homotopy analysis method (HAM) leads to the solutions development. Thus initial guesses and auxiliary linear operators are

$$\tilde{f}_0(\xi) = A(1 - \exp(-\xi)),
 \tag{30}$$

$$\tilde{g}_0(\xi) = \exp(-\xi),
 \tag{31}$$

$$\tilde{\theta}_0(\xi) = \exp(-\xi),
 \tag{32}$$

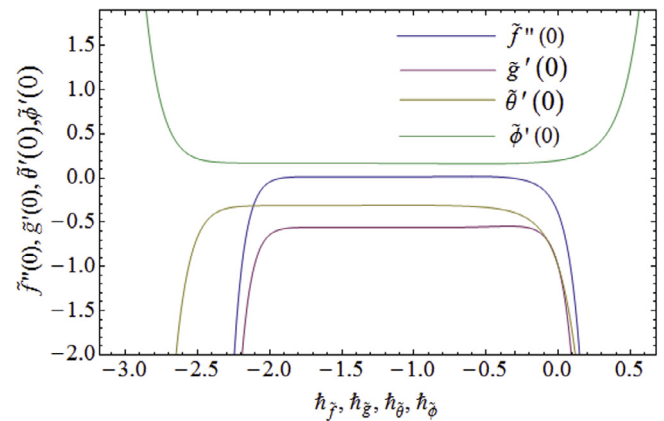


Fig. 2. h -curves for $\tilde{f}''(0), \tilde{g}'(0), \tilde{\theta}'(0)$ and $\tilde{\phi}'(0)$.

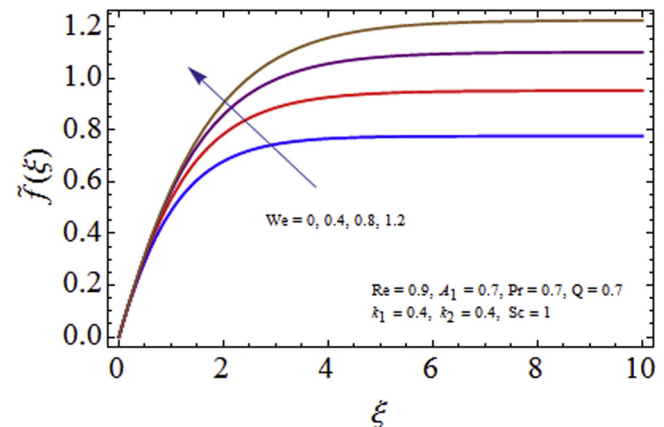


Fig. 3. Impact of We for $\tilde{f}(\xi)$.

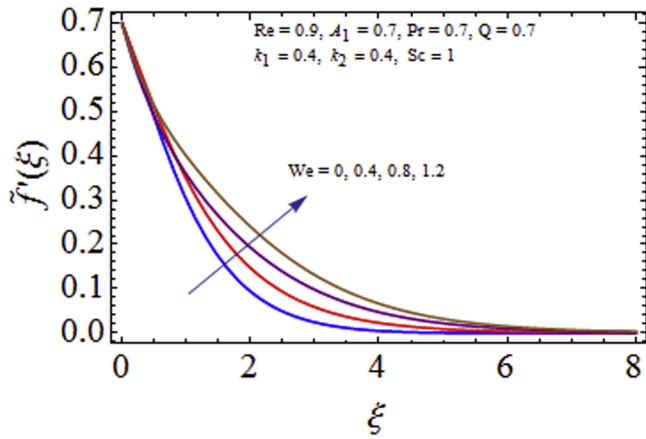


Fig. 4. Impact of We for $\tilde{f}'(\xi)$.

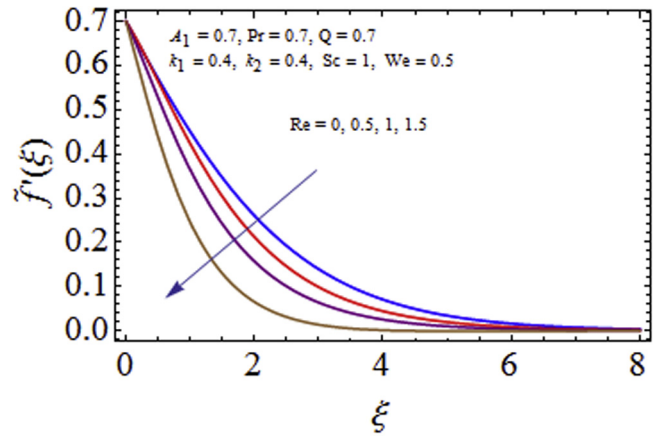


Fig. 7. Impact of Re for $\tilde{f}'(\xi)$.

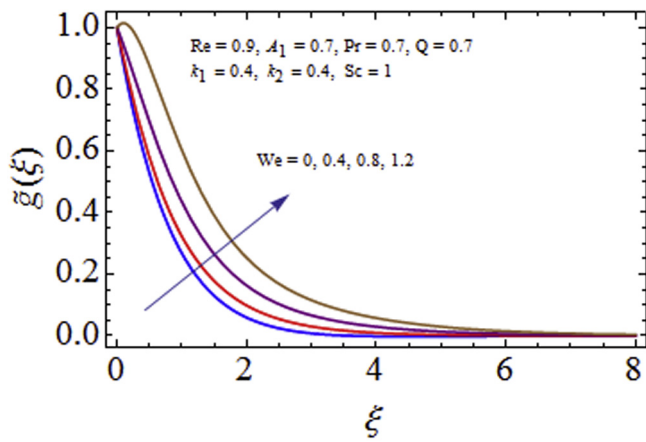


Fig. 5. Impact of We for $\tilde{g}(\xi)$.

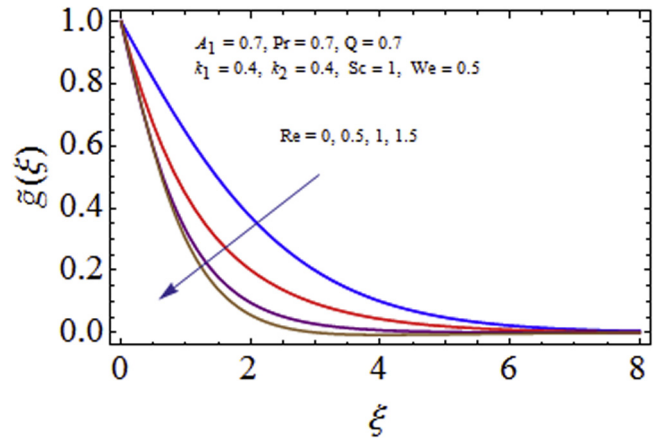


Fig. 8. Impact of Re for $\tilde{g}(\xi)$.

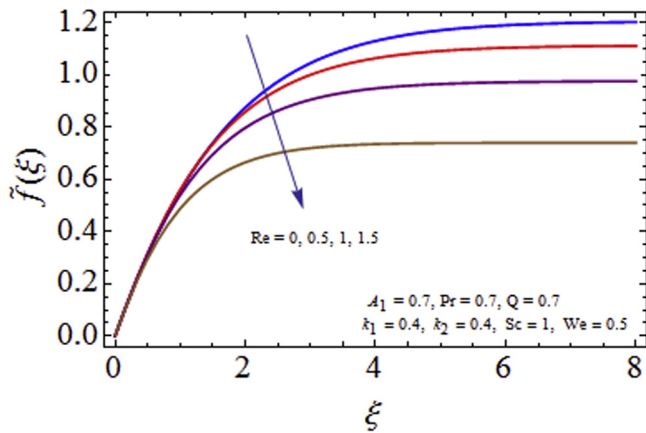


Fig. 6. Impact of Re for $\tilde{f}(\xi)$.

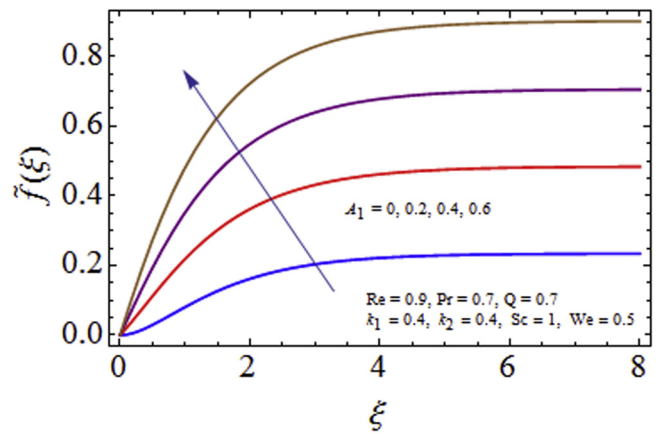


Fig. 9. Impact of A_1 for $\tilde{f}(\xi)$.

$$\tilde{\phi}_0(\xi) = 1 - \frac{1}{2} \exp(-k_2 \xi), \tag{33}$$

$$\mathcal{L}_{\tilde{f}} = \tilde{f}''' - \tilde{f}', \mathcal{L}_{\tilde{g}} = \tilde{g}'' - \tilde{g}, \mathcal{L}_{\tilde{\theta}} = \tilde{\theta}'' - \tilde{\theta}, \mathcal{L}_{\tilde{\phi}} = \tilde{\phi}'' - \tilde{\phi}, \tag{34}$$

with

$$\mathcal{L}_{\tilde{f}} [A_1 + A_2 e^\xi + A_3 e^{-\xi}] = 0, \tag{35}$$

$$\mathcal{L}_{\tilde{g}} [A_4 e^\xi + A_5 e^{-\xi}] = 0, \tag{36}$$

$$\mathcal{L}_{\tilde{\theta}} [A_6 e^\xi + A_7 e^{-\xi}] = 0, \tag{37}$$

$$\mathcal{L}_{\tilde{\phi}} [A_8 e^\xi + A_9 e^{-\xi}] = 0, \tag{38}$$

where A_i ($i = 1 - 9$) are the constants. There is no doubt that series solutions involve auxiliary parameters h_f, h_g, h_θ and h_ϕ . To acquire the admissible ranges we have drawn the h -curves at 16th order of

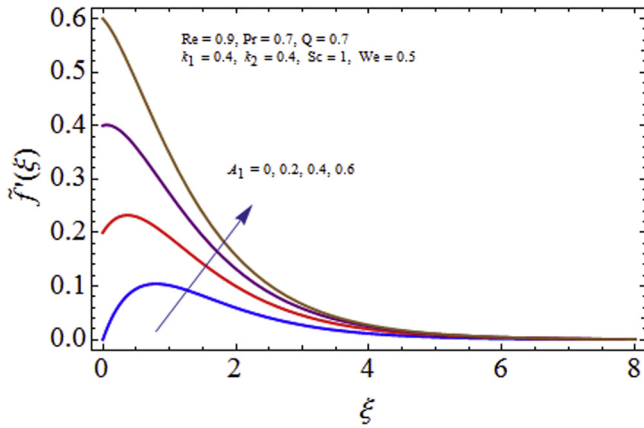


Fig. 10. Impact of A_1 for $\tilde{f}'(\xi)$.

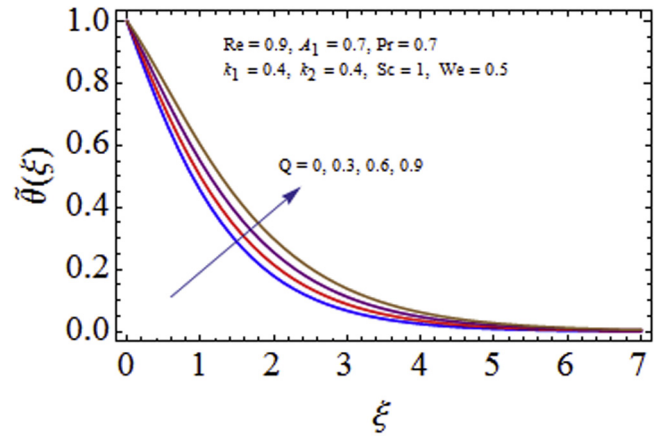


Fig. 13. Impact of Q for $\tilde{\theta}(\xi)$.

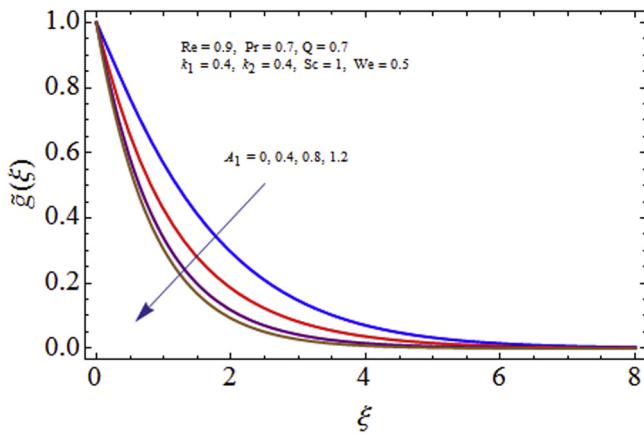


Fig. 11. Impact of A_1 for $\tilde{g}(\xi)$.

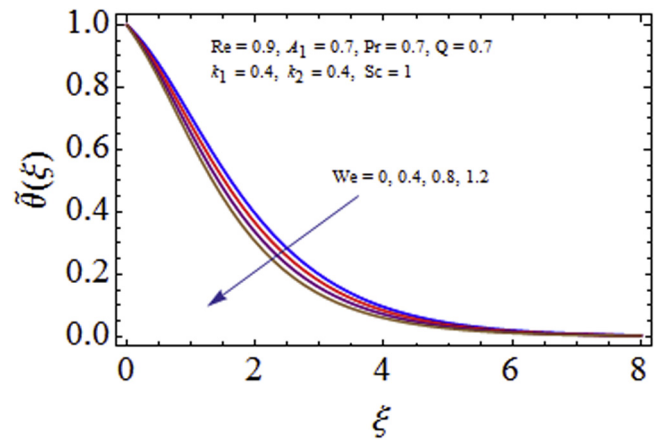


Fig. 14. Impact of We for $\tilde{\theta}(\xi)$.

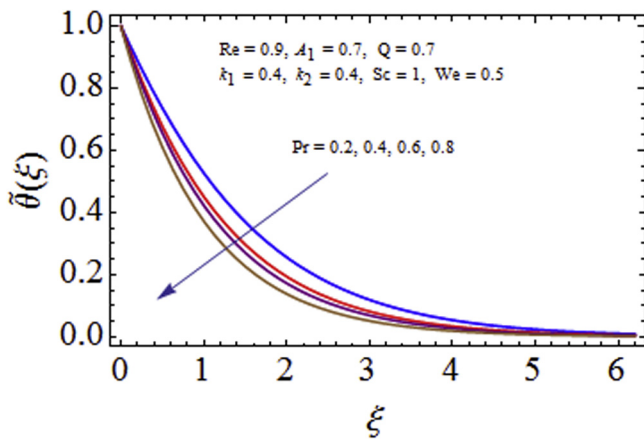


Fig. 12. Impact of Pr for $\tilde{\theta}(\xi)$.

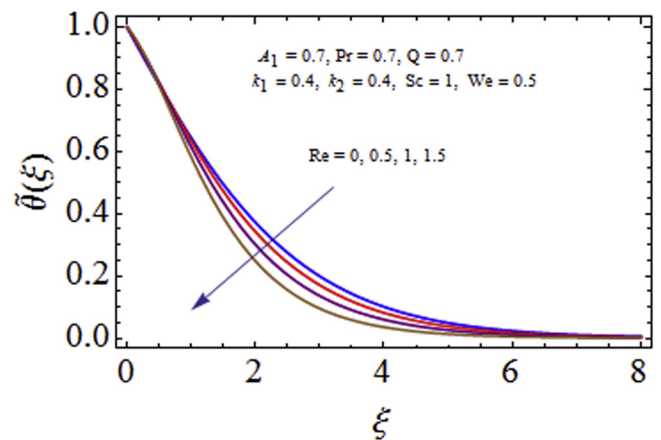


Fig. 15. Impact of Re for $\tilde{\theta}(\xi)$.

approximations. Convergence regions are $-1.9 \leq h_f \leq -0.9$, $-1.8 \leq h_g \leq -0.6$, $-1.5 \leq h_\theta \leq -0.9$ and $-2.3 \leq h_\phi \leq -1.3$ (see Fig. 2). Solution is convergent for entire region of $\xi(0 \leq \xi \leq \infty)$ when $h_f = h_g = -1.5 = h_\phi$ and $h_\theta = -1.3$. Table 1 is constructed to show the order of convergence. $\tilde{f}''(0)$, $\tilde{g}'(0)$, $\tilde{\theta}'(0)$ and $\tilde{\phi}'(0)$ converge at 10th, 23th, 26th and 24th order of approximations respectively.

Discussion

Present section is prepared just to investigate the effects of involved dimensionless variables on velocity (axial, radial, tangential), temperature, concentration, skin friction coefficient and Nusselt number.

0.1. Axial, radial and tangential velocity components

Impact of viscoelastic parameter We on axial, radial and tangential velocity profiles is shown in Figs. 3–5. For larger values of We fluid viscosity decreases because We is inversely proportional to the viscosity and hence fluid velocity (axial, radial and tangential) enhances. Influence of Re on axial, radial and tangential velocities is shown in Figs. 6–8. It is clear from these figures that for larger Reynolds number Re the axial, radial and tangential velocities are reducing. In fact Re is directly proportional to the density of fluid. When density enhances then velocities in radial, axial and tangential directions decay. Figs. 9–11 are portrayed to show the behavior of axial $\tilde{f}(\xi)$, radial $\tilde{f}'(\xi)$ and tangential $\tilde{g}(\xi)$ velocities for stretching parameter A_1 . Magnitude of $\tilde{f}(\xi)$ and $\tilde{f}'(\xi)$ enhances for larger A_1 because stretching rate of disk is increasing through A_1 (see Figs. 9 and 10). Decreasing behavior is observed for tangential velocity $\tilde{g}(\xi)$ with an increase in stretching parameter A_1 . With increase in A_1 the rotational velocity Ω_1 is reduced. It causes decrease in tangential velocity (see Fig. 11).

0.2. Temperature profile

Figs. 12–15 are made to examine the temperature profile. Temperature for Prandtl number Pr is shown in Fig. 12. Larger Pr gradually decreases the temperature of fluid because thermal diffusivity decays for larger Pr . Fig. 13 shows influence of heat source/sink parameter Q on $\tilde{\theta}(\xi)$. It shows that $\tilde{\theta}(\xi)$ is increasing

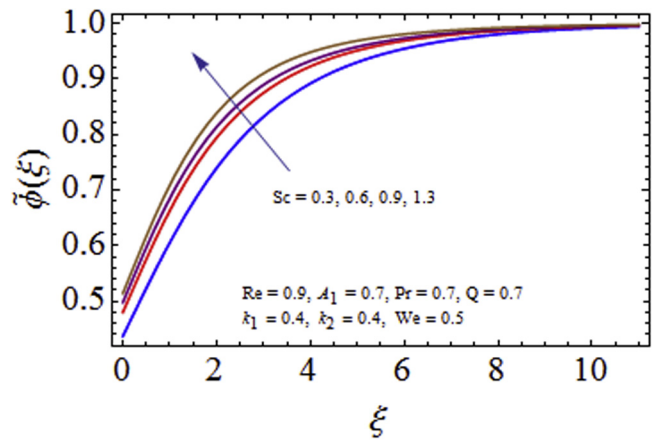


Fig. 18. Impact of Sc for $\tilde{\phi}(\xi)$.

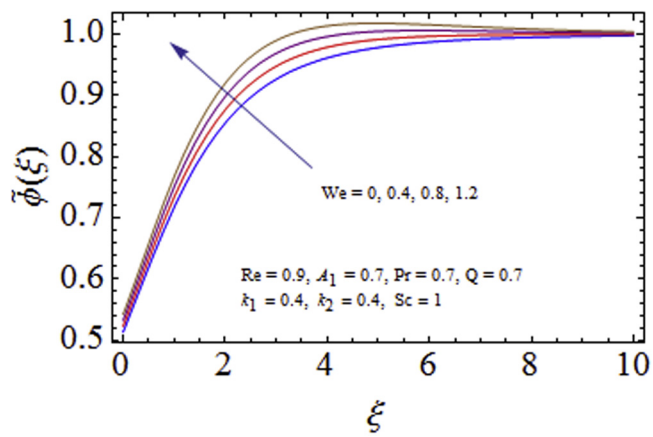


Fig. 19. Impact of We for $\tilde{\phi}(\xi)$.

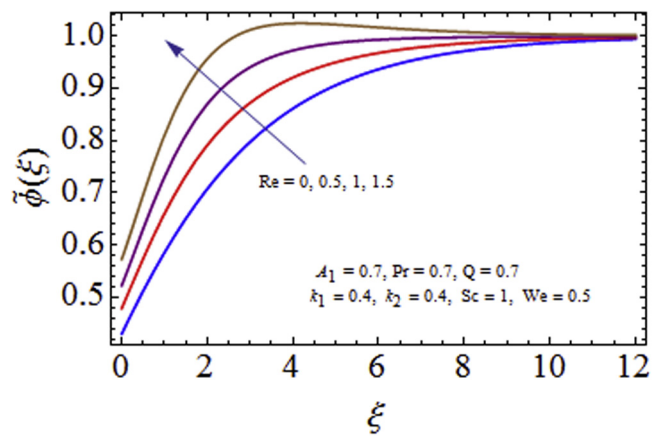


Fig. 20. Impact of Re for $\tilde{\phi}(\xi)$.

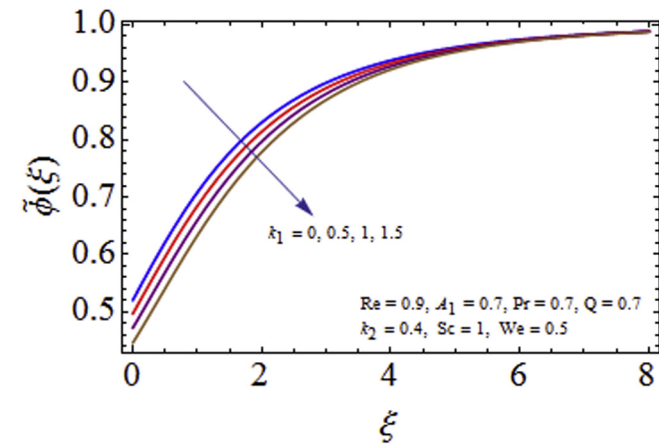


Fig. 16. Impact of k_1 for $\tilde{\phi}(\xi)$.

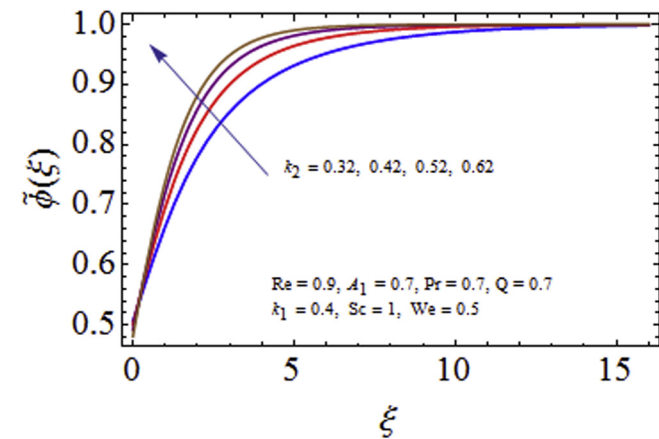


Fig. 17. Impact of k_2 for $\tilde{\phi}(\xi)$.

function of Q . Impact of viscoelastic parameter We on temperature is depicted in Fig. 14. Here decreasing effects are captured for larger We . For larger Reynolds number Re there is decreasing impact of temperature (see Fig. 15).

0.3. Concentration profile

Figs. 16–20 are portrayed to show the influence of involved parameters on concentration profile. Impact of homogeneous reaction parameter k_1 is depicted in Fig. 16. As expected the concentra-

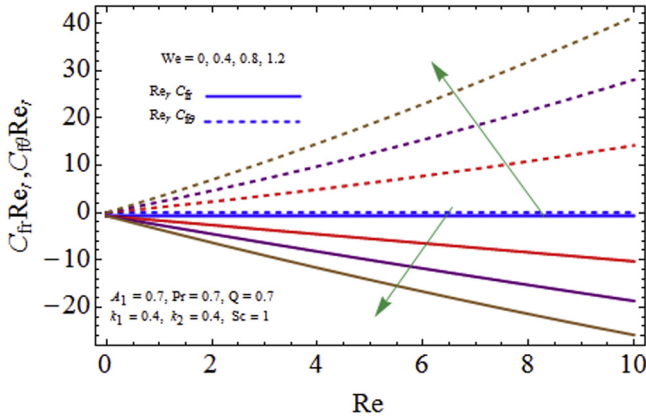


Fig. 21. Impact of We for $C_{fr}Re_\gamma$ and $C_{f\theta}Re_\gamma$.

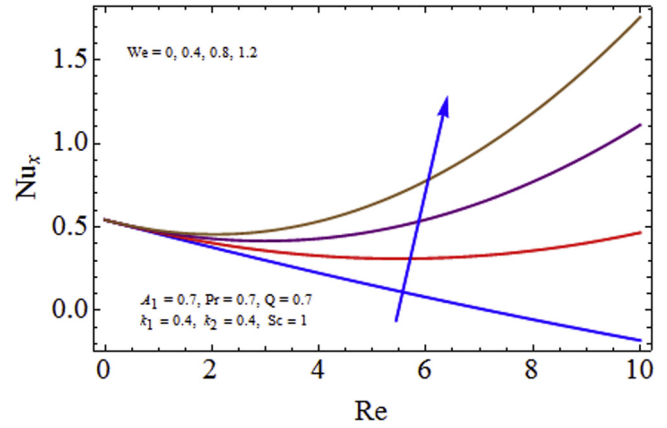


Fig. 24. Impact of We on Nu_x .

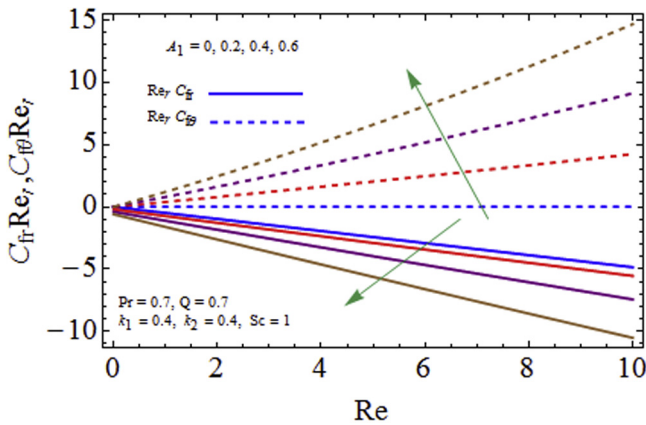


Fig. 22. Impact of A_1 for $C_{fr}Re_\gamma$ and $C_{f\theta}Re_\gamma$.

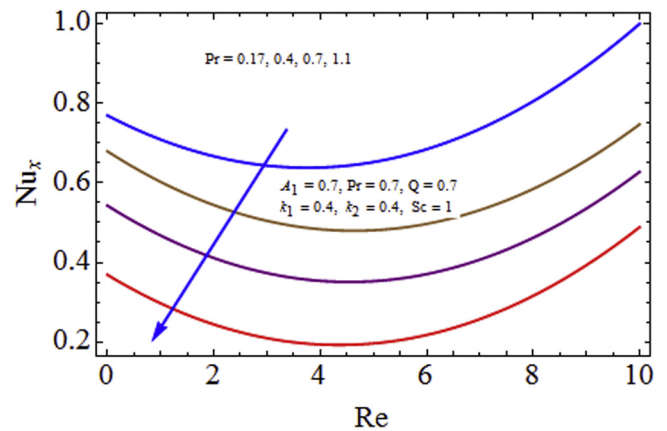


Fig. 25. Impact of Pr on Nu_x .

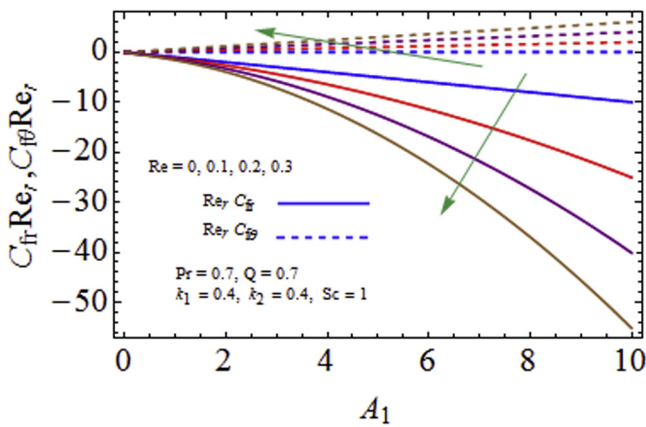


Fig. 23. Impact of Re for $C_{fr}Re_\gamma$ and $C_{f\theta}Re_\gamma$.

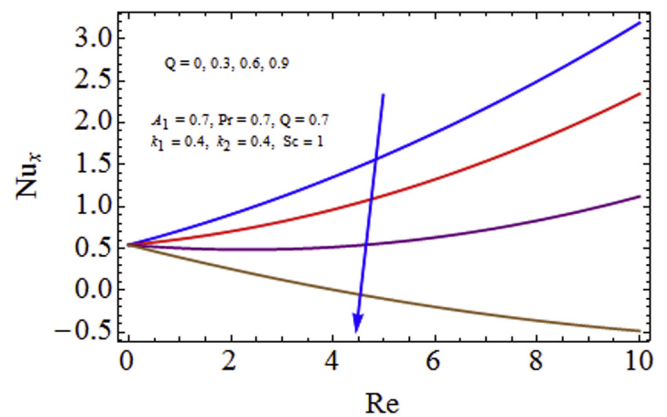


Fig. 26. Impact of Q on Nu_x .

tion of fluid decays with an increase in k_1 . It is through the fact that reactants are consumed during the homogeneous reaction. While opposite behavior of $\bar{\phi}(\xi)$ is captured for larger heterogeneous reaction parameter k_2 (see Fig. 17). For increasing value of k_2 the diffusion coefficient reduces and less diffused particles enhance the concentration. Increment in concentration profile is noticed for larger Sc (see Fig. 18). As Sc is the ratio of momentum to mass diffusivity. Therefore momentum diffusivity enhances for larger Sc which in turn enhances the concentration profile. Fig. 19 shows that for larger We the concentration of fluid increases. Fig. 20 is

portrayed to show the influence of Re on concentration profile. It shows that $\bar{\phi}(\xi)$ enhances with increase in Re .

0.4. Surface drag force

Impact of viscoelastic parameter We , stretching parameter A_1 and Reynolds number Re on skin friction coefficient are shown in Figs. 21–23. It is clear from the Figs. that magnitude of skin friction coefficient in radial and tangential directions enhances for larger We, A_1 and Re .

0.5. Nusselt number

Figs. 24–26 are sketched to analyze the effect of viscoelastic parameter We , Prandtl number Pr and heat generation/absorption parameter Q on Nusselt number. Fig. 24 shows that Nusselt number is increasing function of We while reduction in heat transfer rate is noticed for larger Prand Q (see Figs. 25 and 26).

Closing remarks

Here we consider the flow of second grade fluid accounting heat source/sink and homogeneous-heterogeneous reactions. The main findings are:

- Increasing behavior of axial, radial and tangential velocities is captured for larger viscoelastic parameter We .
- Temperature profile decreases for larger Prandtl number Pr while opposite behavior is noticed for increasing heat source/sink parameter Q .
- Temperature profile is decreasing function of viscoelastic parameter We .
- Concentration profile decays for larger k_1 while opposite behavior is examined for increasing k_2 .
- Concentration profile shows similar behavior for larger Schmidt number Sc and viscoelastic parameter We .
- Viscoelastic parameter We give rise to surface drag force and Nusselt number.
- Heat transfer rate decays for larger Prandtl number Pr .

References

- [1] Hayat T, Qayyum S, Alsaedi A, Shehzad SA. Nonlinear thermal radiation aspects in stagnation point flow of tangent hyperbolic nanofluid with double diffusive convection. *J Mol Liq* 2016;223:969–78.
- [2] Turkyilmazoglu M. Flow of a micropolar fluid due to a porous stretching sheet and heat transfer. *Int J Non-Linear Mech* 2016;83:59–64.
- [3] Hayat T, Qayyum S, Imtiaz M, Alsaedi A. Three-dimensional rotating flow of Jeffrey fluid for Cattaneo-Christov heat flux model. *AIP Adv* 2016;6(2):025012.
- [4] Rahman SU, Ellahi R, Nadeem S, Zia QMZ. Simultaneous effects of nanoparticles and slip on Jeffrey fluid through tapered artery with mild stenosis. *J Mol Liq* 2016;218:484–93.
- [5] Hayat T, Waqas M, Khan MI, Alsaedi A. Impacts of constructive and destructive chemical reactions in magnetohydrodynamic (MHD) flow of Jeffrey liquid due to nonlinear radially stretched surface. *J Mol Liq* 2016;225:302–10.
- [6] Das K, Sharma RP, Sarkar A. Heat and mass transfer of a second grade magnetohydrodynamic fluid over a convectively heated stretching sheet. *J Comp Des Eng* 2016;3:330–6.
- [7] Hayat T, Jabeen S, Shafiq A, Alsaedi A. Radiative squeezing flow of second grade fluid with convective boundary conditions. *PLoS One* 2016;11(4):e0152555.
- [8] Majeed A, Javed T, Ghaffari A. Numerical investigation on flow of second grade fluid due to stretching cylinder with Soret and Dufour effects. *J Mol Liq* 2016;221:878–84.
- [9] Hayat T, Zubair M, Waqas M, Alsaedi A, Ayub M. Application of non-Fourier heat flux theory in thermally stratified flow of second grade liquid with variable properties. *Chin J Phys* 2017;55:230–41.
- [10] Ariel PD. Computation of flow of a second grade fluid near a rotating disk. *Int J Eng Sci* 1997;35:1335–57.
- [11] Karman TV. Über laminare and turbulente Reibung. *Zeit Angew Math Mech* 1921;1:233–52.
- [12] Cochran WG. The flow due to a rotating disk. *Proc Camb Philos Soc* 1934;30:365–75.
- [13] Stewartson K. On the flow between two rotating coaxial disks. *Proc Comb Philos Soc* 1953;49:333–41.
- [14] Chapple PJ, Stokes VK. On the flow between a rotating and a stationary disk. Report No. FLD 8. Dept. Mech. Eng. Princeton University; 1962.
- [15] Hayat T, Qayyum S, Imtiaz M, Alsaedi A. Flow between two stretchable rotating disks with Cattaneo-Christov heat flux model. *Result Phys* 2017;7:126–33.
- [16] Ellahi R, Tariq MH, Hassan M, Vafai K. On boundary layer nano-ferroliquid flow under the influence of low oscillating stretchable rotating disk. *J Mol Liq* 2016 (in press).
- [17] Hayat T, Qayyum S, Imtiaz M, Alsaedi A. MHD flow and heat transfer between coaxial rotating stretchable disks in a thermally stratified medium. *PLoS One* 2016;11(5):e0155899.
- [18] Raju CSK, Sandeep N. MHD slip flow of a dissipative Casson fluid over a moving geometry with heat source/sink: a numerical study. *Acta Astronaut* 2017;133:436–43.
- [19] Das K, Acharya N, Kundu PK. The onset of nanofluid flow past a convectively heated shrinking sheet in presence of heat source/sink: a Lie group approach. *Appl Therm Eng* 2016;103:38–46.
- [20] Hayat T, Qayyum S, Alsaedi A, Shafiq A. Inclined magnetic field and heat source/sink aspects in flow of nanofluid with nonlinear thermal radiation. *Int J Heat Mass Transfer* 2016;103:99–107.
- [21] Noor NFM, Abbasbandy S, Hashim I. Heat and mass transfer of thermophoretic MHD flow over an inclined radiate isothermal permeable surface in the presence of heat source/sink. *Int J Heat. Mass Transfer* 2012;55:2122–8.
- [22] El-Aziz MA. Dual solutions in hydromagnetic stagnation point flow and heat transfer towards a stretching/shrinking sheet with non-uniform heat source/sink and variable surface heat flux. *J Egypt Math Soc* 2016;24:479–86.
- [23] Hayat T, Khan MI, Alsaedi A, Khan MI. Homogeneous-heterogeneous reactions and melting heat transfer effects in the MHD flow by a stretching surface with variable thickness. *J Mol Liq* 2016;223:960–8.
- [24] Imtiaz M, Hayat T, Alsaedi A. MHD convective flow of Jeffrey fluid due to a curved stretching surface with homogeneous-heterogeneous reactions. *PLoS One* 2016;11(9):e0161641.
- [25] Abbas Z, Sheikh M, Pop I. Stagnation-point flow of a hydromagnetic viscous fluid over stretching/shrinking sheet with generalized slip condition in the presence of homogeneous-heterogeneous reactions. *J Taiwan Inst Chem Eng* 2015;55:69–75.
- [26] Kameswarana PK, Shawa S, Sibanda P, Murthy PVS. Homogeneous-heterogeneous reactions in a nanofluid flow due to a porous stretching sheet. *Int J Heat Mass Transfer* 2013;57:465–72.
- [27] Sheikh M, Abbas Z. Homogeneous-heterogeneous reactions in stagnation point flow of Casson fluid due to a stretching/shrinking sheet with uniform suction and slip effects. *Ain Shams Eng J* 2015;4 (in press).
- [28] Hayat T, Qayyum S, Imtiaz M, Alsaedi A. Impact of Cattaneo-Christov heat flux in Jeffrey fluid flow with homogeneous-heterogeneous reactions. *PLoS One* 2016;11(2):e0148662.
- [29] Sui J, Zheng L, Zhang X, Chen G. Mixed convection heat transfer in power law fluids over a moving conveyor along an inclined plate. *Int J Heat Mass Transfer* 2015;85:1023–33.
- [30] Hayat T, Khan MI, Farooq M, Alsaedi A, Waqas M, Yasmeen T. Impact of Cattaneo-Christov heat flux model in flow of variable thermal conductivity fluid over a variable thicked surface. *Int J Heat Mass Transfer* 2016;99:702–10.
- [31] Hayat T, Khan MI, Farooq M, Yasmeen T, Alsaedi A. Stagnation point flow with Cattaneo-Christov heat flux and homogeneous-heterogeneous reactions. *J Mol Liq* 2016;220:49–55.
- [32] Hayat T, Qayyum S, Imtiaz M, Alsaedi A, Alzahrani F. Partial slip effect in flow of magnetite- Fe_3O_4 nanoparticles between rotating stretchable disks. *J Magn Magn Mater* 2016;413:39–48.
- [33] Turkyilmazoglu M. An effective approach for evaluation of the optimal convergence control parameter in the homotopy analysis method. *Filomat* 2016;30:1633–50.
- [34] Khan MI, Waqas M, Hayat T, Alsaedi A. A comparative study of Casson fluid with homogeneous-heterogeneous reactions. *J Colloid Interface Sci* 2017;498:85–90.
- [35] Hayat T, Khan MI, Farooq M, Alsaedi A, Yasmeen T. Impact of Marangoni convection in the flow of carbon-water nanofluid with thermal radiation. *Int J Heat Mass Transfer* 2017;106:810–5.
- [36] Hayat T, Qayyum S, Imtiaz M, Alsaedi A. Radiative flow due to stretchable rotating disk with variable thickness. *Results Phys* 2017;7:156–65.